Conference Proceedings

Solar World Congress 2015
Daegu, Korea, 08 – 12 November 2015

Development of a Solarized Rotary Kiln for High-Temperature Chemical Processes

Lucia Arribas[1], Veselin Miroslavov[1], Selvan Bellan[1], Manuel Romero[1], Jose Gonzalez-Aguilar[1]

[1]Unit of High Temperature Processes, IMDEA Energy Institute, E-28935, Mostoles (Spain)

Abstract

This work presents the design, characterization and commissioning of a directly-irradiated solar rotary reactor, which can be used for multiple applications such as chemical reactions (solar chemistry), thermochemical process or studies about mechanical strength and attrition of different materials, focusing on thermochemical reactions of manganese oxide. The main features of the reactor and test bed are as follows: samples are directly irradiated by concentrated radiation provided by a 7kWe high-flux solar simulator (HFSS) and a rotating cavity that promotes good mass and heat transfer, as well as high surface area for the reactions. Optical simulations and CFD analysis show that 1 kW of incident power and 1700 K can be achieved at the reaction zone, which is located at the secondary focus of the high-flux solar simulator. Manganese oxide cylindrical pellets (85% Mn_3O_4, 15% Mn_2O_3, mean particle size 3.5 mm) are used to perform the thermochemical reactions. X-Ray Diffraction is used to analyze the pellets composition before and after the test. A full conversion of the initial 15% of Mn_2O_3 is achieved.

Keywords: *solar reactors, solar simulator, rotary kiln, manganese oxide*

1. Introduction

Enhance the renewable energy contribution to the global energy mix is necessary in order to reduce global warming. Generally, however, the main disadvantage of some renewable resources such as solar or wind is their lack of dispatchability, since their production depends on transient weather conditions. For the generated renewable energy to be used when it is needed, it should be either stored or transformed into another type of fuel.

Short-to-long term thermal storage can be achieved using concentrated solar energy with the addition of thermal storage, thermochemical storage or by producing solar fuels such as hydrogen; which makes possible to implement high-flexible dispatching strategies. Recent studies focus on thermochemical storage and solar fuels (Romero and Steinfeld, 2012). Both processes are based on the use of concentrated solar radiation, which requires adequate optical concentration systems and optimized solar reactors that are capable to withstand high temperatures, where thermal losses are minimized, and which favor mass and heat transfer (Alonso and Romero, 2015).

Solar reactors are classified into directly and indirectly heated reactors, depending on whether particles are directly irradiated or not. Particle reactors can be in turn classified into stacked, fluidized or suspended, and entrained bed configurations. This paper will focus on a rotary kiln that functions as a stacked bed and a brewed oven.

Advantages of a rotary kiln are that they produce relatively low radiation heat losses and uniformly high temperatures, and that the reactive material can be directly irradiated, which leads to intensive heat and mass transfer (Tescari et al., 2013). However, they present technical disadvantages associated with the presence of moving parts, such as the complexity of achieving a balanced rotation, sealing the structure and measuring temperatures inside the rotating tube.

A number of rotary solar reactors have been already employed in research. The Roca reactor (Haueter et al.,

doi:10.18086/swc.2015.04.10 Available at http://proceedings.ises.org

1999), commissioned at the Paul Scherrer Institute (PSI), is a solar rotary reactor of 10 kW designed to produce the thermal reduction of zinc oxide (ZnO) into zinc (Zn) and oxygen (O_2). The Zirrus reactor (Müller et al., 2006), also designed at the PSI to reduce zinc oxide, consisted of a rotating cavity where centripetal acceleration forced the reactant ZnO to cover the cavity wall. Unlike Roca, where the ZnO was both the reactant and the insulating material, these two functions were decoupled in the Zirrus. Thus, the Zirrus reactor was composed of an inner cavity wall impermeable to gas diffusion, but capable of functioning at the decomposition temperature of ZnO in a corrosive environment containing ZnO, gaseous Zn and O_2.

A rotary reactor that produced lime by calcination of calcite was tested in the solar furnace of PSI (Meier et al., 2004). This 10-kW reactor was basically a rotary kiln of 600 mm length and 350 mm diameter, operated horizontally and in a continuous mode. The raw material was stored in a hopper that is placed on top of the rear part of the reactor. The rotation speed was between 2-7 rpm.

A rotary reactor by the German Aerospace Center (DLR) for solar thermochemical energy storage (Neises et al., 2012) was used to perform the reduction of cobalt (II, III) oxide to cobalt (II) oxide and O_2. The total flow used was between 4-8 l/min and a maximum rotational speed of 6 rpm was achieved.

Recently, a rotary reactor for thermochemical energy storage with copper oxide was tested in the solar furnace HoSIER at UNAM, Mexico (Alonso et al., 2015). The reactor body, including the stainless steel housing and an insulation layer of porous alumina, was stationary. Only the reaction chamber rotated around a central axis, connected to an engine at the back of the reactor. The reaction chamber was a rotary cylinder made out of alumina, with an inner diameter of 57.5 mm, an outer diameter of 67 mm and a length of 74 mm. Typical operating conditions were a volumetric flow rate of 10 l/min and rotational speed of 4 rpm.

2. Reactor design and experimental setup

The objective of the reactor design is to get a versatile device that can be used in different processes without many changes. Examples of applications are chemical reactions (solar thermochemistry), thermochemical processes or studies about mechanical strength and/or attrition of different materials. Specifically, this work presents the reduction of manganese oxide (Mn_3O_4). The reactor is presented in Fig. 1 and is composed of the following elements:

A reacting cavity which consists of a fixed conical aperture with a large enough aperture for the incoming radiation (an upper diameter of 11 cm, a lower diameter of 38 mm and a height of 80 mm), and a rotary tube of alumina (with an outer diameter of 45 mm, an inner diameter of 35 mm, and a length of 500 mm). The axial rotation of the tube produces homogeneous temperature, and high mass and heat transfer in the reaction zone. To minimize heat losses, ceramics bricks are used as insulation.

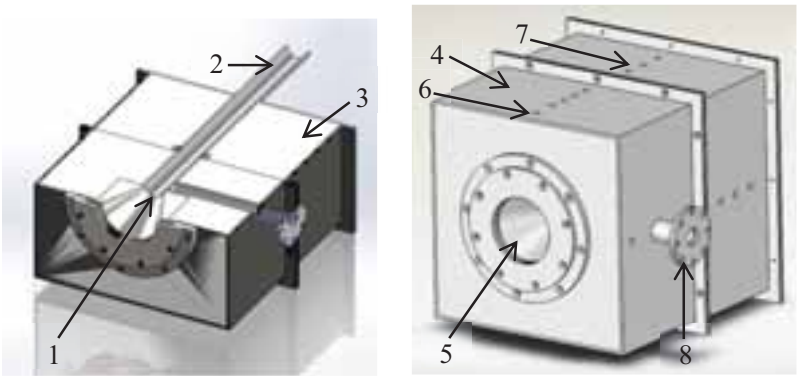

Fig. 1: Scheme of rotary kiln. (1) Cavity; (2) rotary tube of alumina; (3) ceramics bricks; (4) stainless steel housing; (5) quartz glass window; (6) gas inlet; (7) thermocouples places; (8) window for pyrometer

As working in a controlled atmosphere is desirable, air tightness is necessary. To achieve it, the reactor has an external housing of stainless steel, where measuring instrumentation is also located, and a quartz window of high transmittance that allows particles to be directly irradiated and seals the cavity. This window should be clean during experiments, thus the gas feeding is performed by four gas inlets located at the lateral wall of the reactor. The external dimensions of the reactor are 40x35x35 cm^3. 28 K-type thermocouples are installed at different axial and radial distances, and two inside the tube. A window has been included in one of the lateral walls of the facility in order to measure temperatures with a pyrometer. An electric motor rotating at 1390 rpm is employed to move the tube at approximately 92 rpm (9.63 rad/s) through a 1/15 reducer.

Two photographs of the rotary kiln are showed in Fig. 2, where it is possible see the final setup. The axis of rotation is fixed by two treads, one at back cover of the housing and another at gas outlet, behind the gear. Instruments devices installed are the following: a relative pressure transducer at gas inlet; a pressure drop transducer between inlet and outlet; a flowmeter; 30 K-type thermocouples; a pyrometer. All of them connected with data acquisitions cards in order to monitor the course of the experiments by a LabView software. Gas outlet is carried to the gas conditioner and later to the gas analyzer (Siemens Ultramat 23).

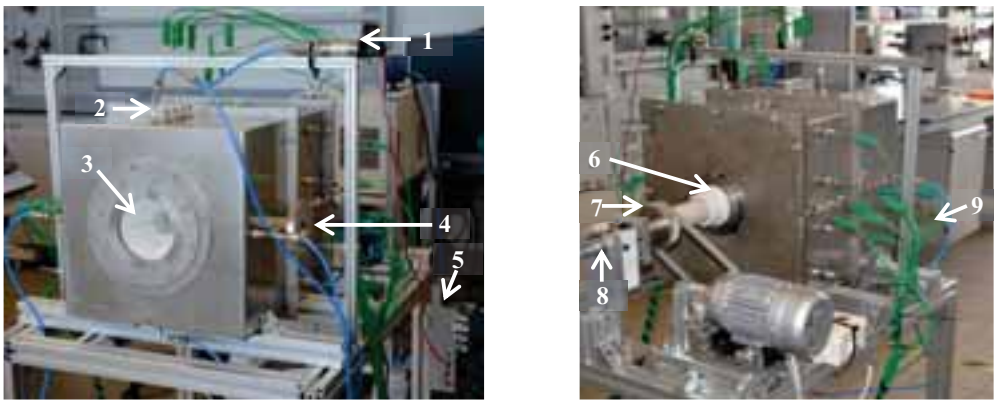

Fig. 2: Front view (left) and back view (right) of rotary kiln. (1) Pressure transducer; (2) gas inlet; (3) window; (4) window for pyrometer; (5) data acquisition card; (6) tread; (7) gear; (8) gas outlet; (9) thermocouples

To avoid particles reaching the conical part, the reactor is tilted 4º with respect to the horizontal and a ceramic ring is placed in the tube inlet. As particles can also move towards the outlet, another ceramic ring was placed at the end of the reaction zone (4 cm behind the inlet), but which did not restrict the gas flow. However, it was observed after the firsts commissioning experiments that some powder still reached the conical part, so the front ceramic ring was replaced by one with a smaller aperture (as shown in Fig. 3).

Fig. 3: Ceramics rings. Front ring was changed after first experiments in order to avoid sample losses

3. Numerical Analysis

In order to characterize the reactor, an optical analysis was conducted using the Monte Carlo Ray-tracing software TracePro 7.2, and the flow was numerically simulated by means of COMSOL Multiphysics 4.4.

The optical analysis aimed at determining the optimal position of the reactor with respect to the high flux solar simulator (HFSS) that maximizes sample temperatures and calculating the radiation distribution in the different parts of the reactor.

The optical system contains the main optical components of the high flux solar simulator, a 7kWe Xenon arc lamp and an ellipsoidal reflector. The lamp arc is located at the first focus of the reflector, and radiation is concentrated at the second focus. The optical model included a light source that accurately describes the arc shape and was obtained from CCD images of real arc discharge (showed in Fig. 4).

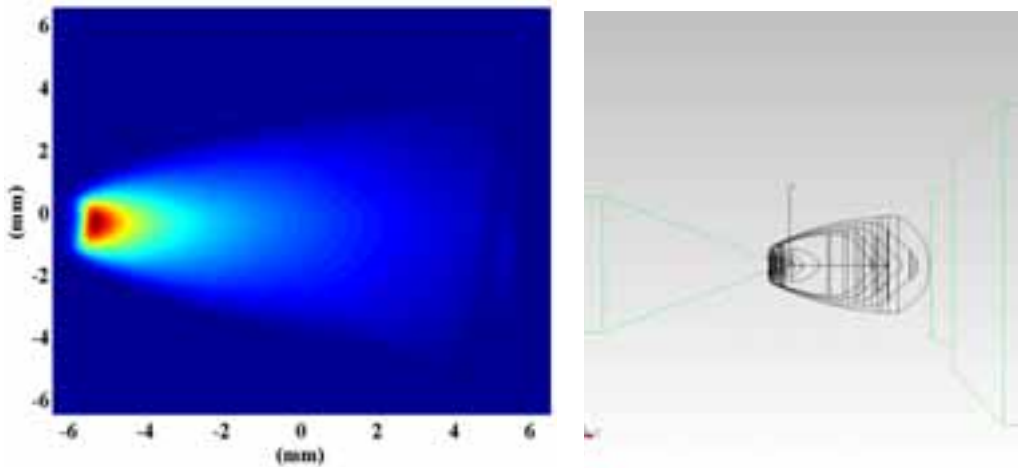

Fig. 4: Discharge arc, CCD image (left) and TracePro model (right)

The definition of the reflector scattering properties was based on the Bidirectional Scattering Distribution Function (BSDF), which consists of measuring the light scattering from a surface in difference directions. For this model, the Elliptical Gaussian BSDF was used.

The number of rays determines simulation times and the resolutions of maps. In order to obtain enough resolution in the simulated maps in reasonable time scales, 139,000 rays were fixed (1000 rays per surface). The total power of the light source was set to 1 kW and results were then scaled according to experimental measurements conducted at the focus.

A square surface (80 mm side length) was located at the focus and rays were traced. The total power in the surface is 443.21 W in the simulations, whereas 1397 W were measured experimentally (Fig. 5), therefore scale factor is 3.15.

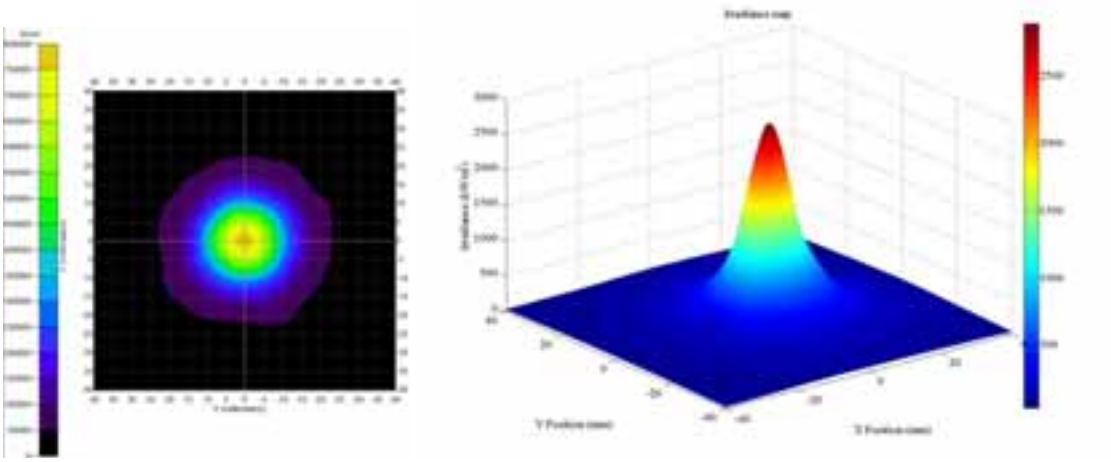

Fig. 5: Radiation measurement at the second focal point, ray tracing (left) and experimentally (right)

The cavity of the reactor (conical part and rotary tube) was implemented by means of gray-body Lambertian surfaces with a 30% absorptance. A schematic of geometry simulated can be seen in Fig. 6. The reactor is inclined 4 degrees with respect to the horizontal. The distance between the secondary focus (target plane) and the central point of the reactor cavity inlet is referred to as *d*. Four cases with different values of *d* were numerically simulated: 5 cm (outside tube), 0 cm (at the tube inlet), and 1 cm and 3 cm inside tube.

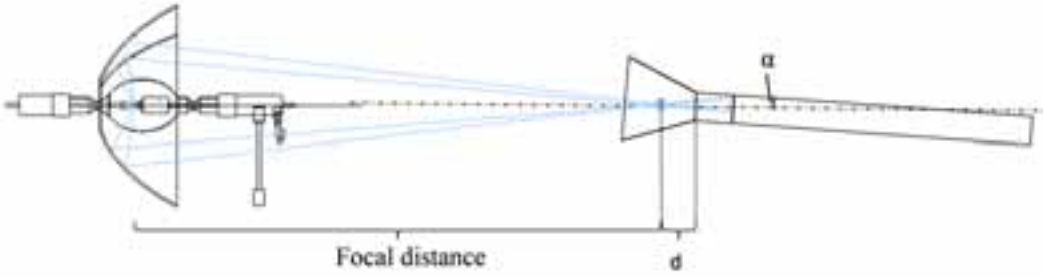

Fig. 6: Scheme of solar simulator and the cavity of the reactor

Results showed that the optimal positions of the reactor with respect to the solar simulator were either when *d* was equal to 0 cm or 1 cm, since the total power at reaction zone was higher than when *d* was equal to 5 cm outside tube and 3 cm inside tube. Table 1 shows the results from simulation with $d = 0$ cm. The total power is around 1 kW at the reaction zone (the first 4 centimeters of the tube), and the stagnation temperature, calculated from Stefan-Boltzmann law with emissivity equal to 1 (ideal radiator), is almost 1750 K.

Irradiance maps of the different parts of the reactor are shown in Figs. 7 and 8 (the latter covering the reaction zone). It can be seen that, from the reactor inlet to the ceramic ring, the maximum power is achieved just in front of the ceramic piece where the sample will be located. Case 2 refers to optical analysis results for ceramic ring with smaller aperture (Fig. 3) performed after experimental tests.

Tab. 1: Total Power at different parts of the reactor obtained by ray tracing, once weighed by real power of the source (2 kW)

Zone	Total Power (W)	Total Power (W) case 2
Cone	1243.59	1745.11
Ring	105.79	819.52
Reaction lower	525.34	101.26
Reaction upper	641.46	114.44
Reaction total	1166.81	215.70

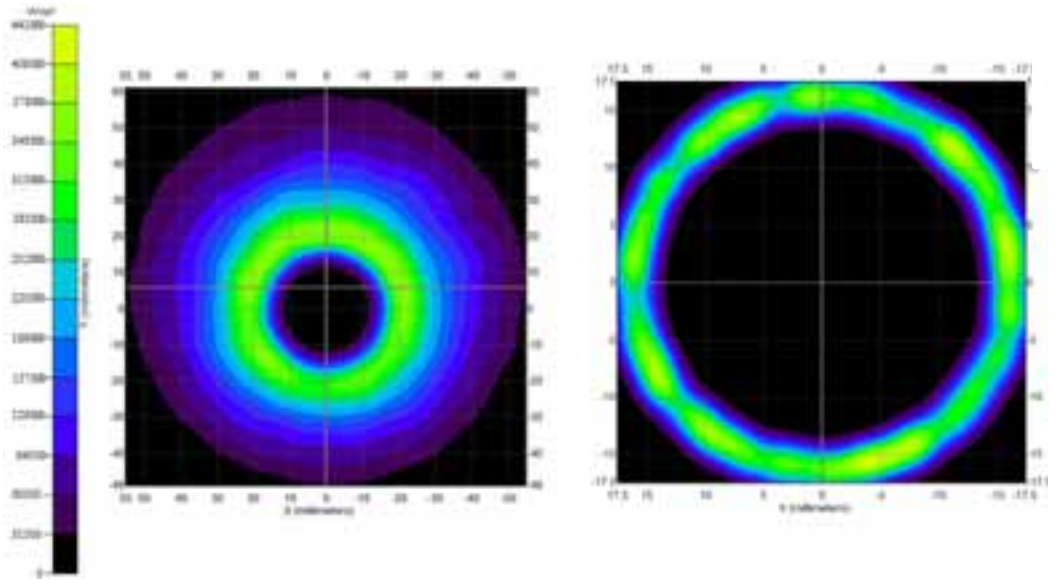

Fig. 7: Irradiance maps: cone (left) and front ring (right)

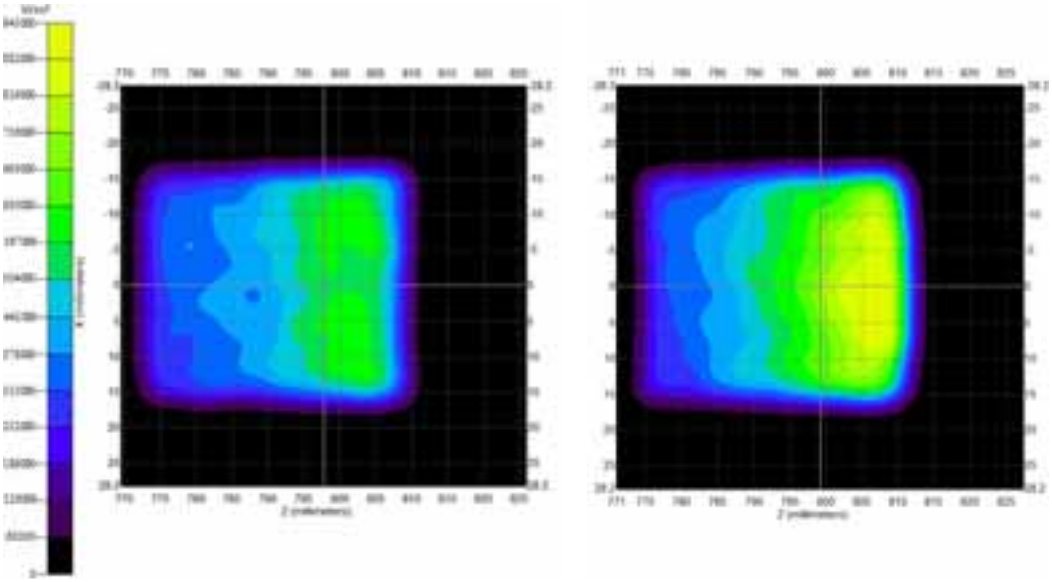

Fig. 8: Irradiance maps: lower half (left) and upper half (right)

The preliminary CFD analysis was conducted to study and assess the flow field and temperature distributions in the reactor. The reactor model was three-dimensional in order to take into account the four flow inlets, which are situated at fixed locations around the circumference. Simulations were thus conducted in one quarter of the geometry (including a flow inlet) in order to reduce the required computational times. Periodic boundary conditions were employed for the flow at the interfaces.

An unstructured mesh was built (with cell growth controlled by the flow physics), with around 65,000 elements. A conjugate heat transfer model was employed.

Boundary conditions of inlet velocity (varying between 1-20 m/s, in the parametric study), outlet pressure (atmospheric) and radiative flux were established. Irradiance variables in both the conical section and the reaction zone were fixed from the ray tracing results and taken as constant values in the simulation. Convective heat transfer between the reactor housing and ambient (at 300 K), and radiative heat transfer between the front window and ambient were simulated.

Figure 9 shows the velocity field in the cavity. As expected, maximum velocities are achieved in the center of the tube. Gas velocity increases along the conical section due to the reduction in the flow cross-sectional area. This enhances the mixing of the gas and avoid reactants deposits on the window.

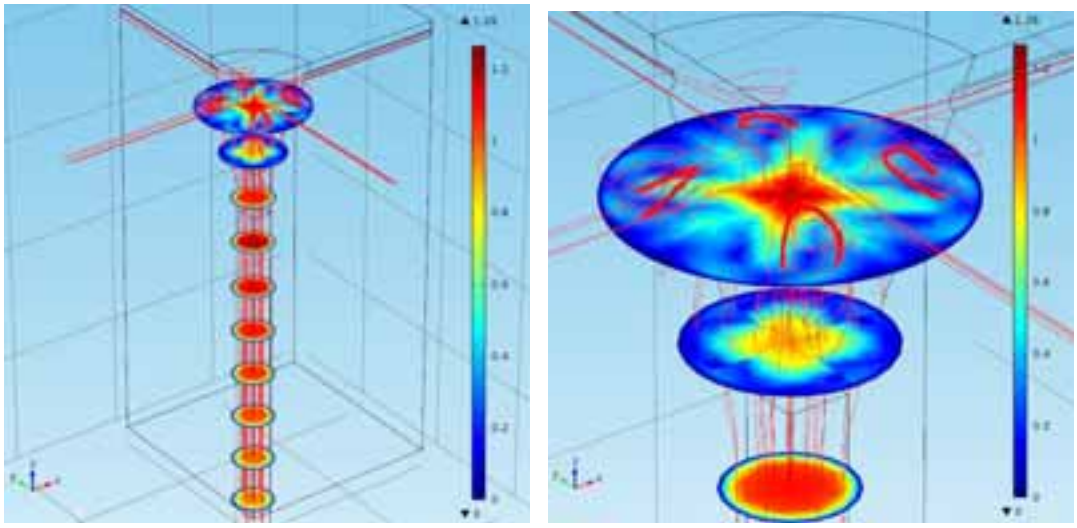

Fig. 9: Velocity field and streamlines at the cavity (left) and cone (right) for gas inlet velocity of 3 m/s (total flow 33 cl/s)

Temperature results are presented in Fig. 10. Maximum temperatures of around 1700 K are achieved in the reaction zone, in agreement with the optical calculations. The housing remains at 300 K, which demonstrates the correct sizing of the insulation. Simulations at higher velocities yield similar fields, with slightly lower temperatures (increasing velocity from 3 to 20 m/s gives a reduction in temperatures of around 50 K), since gas has room temperature at the inlets and cools the reactor more to higher flow (more gas, more convective heat transfer).

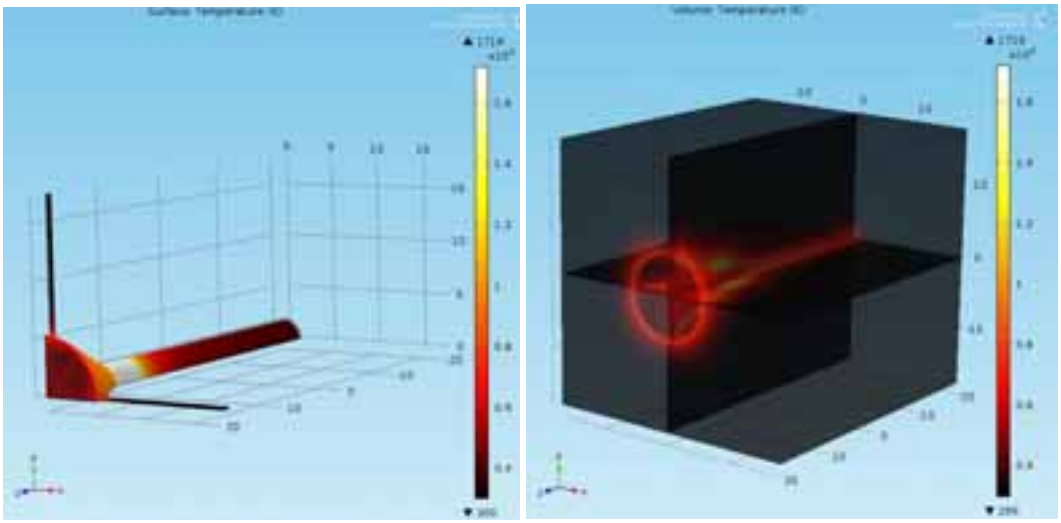

Fig. 10: Temperature distribution of the rotary kiln at a gas inlet velocity of 3 m/s (total flow 33 cl/s)

The evolution of temperature with time in different parts of the reactor is shown in Fig. 11. Temperature increases rapidly in the first minute (high slope), but the rate of change subsequently decreases. Temperatures are practically constant after 20 minutes, except at insulation, which has a much larger thermal inertia.

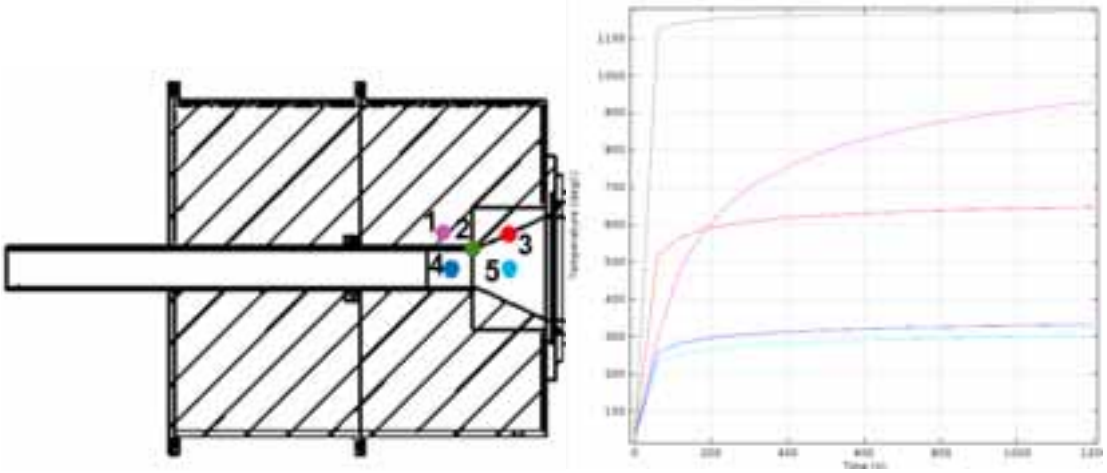

Fig. 11: Scheme of points studied (left) and temperature evolution versus time at those points of the reactor at initial velocities of gas of 3 m/s (total flow 33 cl/s) (right). Points: 1 (pink), 2 (green), 3 (red), 4 (blue), 5 (cyan)

Achieving homogenous temperatures rapidly means that is not necessary introduce rotation in the model with complete geometry of the reactor, since it is possible consider a constant radiation at surface of the tube. When a reactive material is located at the reaction zone, movement helps to get homogenous temperature at the sample and favoring heat and mass transfer with the gas.

Temperatures obtained from CFD results at the reaction zone are similar to the corresponding in experimentation. However, it is necessary improving CFD model in order to approximate it to reality at gas heating.

4. Experimental Results

The objective of the experimental part is the commissioning of the set up. Before the chemical reaction application, the reactor should be experimentally characterized. Firstly, response function of the reactor is determining monitoring evolution of the oxygen concentration at reactor outlet after fast changes in gas composition at reactor inlet. Secondly, an inert sample (silicon carbide) is used to perform thermal characterization in order to know the reactor behavior at high temperature with different irradiance, such as the changes in the reactor materials and maximum temperatures achieve at the different parts of the reactor. Finally, thermochemical reaction of manganese oxide is carried out.

In order to determine the response function, air is fed through the inlets until steady state conditions are established in the working section. It is considered that the steady state is reached when the oxygen concentration becomes stable (it does not change more than 2% in 3 minutes). At this point, the air feed is changed from air to nitrogen and the transient measurements of the oxygen concentration are analyzed (shown in Fig. 12). First, 66 seconds are necessary for the first nitrogen atoms to reach the location where gas is analyzed. Afterwards, the decrease in oxygen concentration approximately follows a negative exponential function, $\exp(-t/t_m)$, with a time constant of $t_m = 51$ seconds (the time constant has been taken as the time at which 63.21% of the total decrease has occurred).

Thermal characterization was conducted with the HFSS. An alumina screen was placed in front of the reactor as thermal shield to protect the external housing from the intense radiation (as shown in Fig. 13).

An inert silicon carbide sample was used in the first series of experiments to conduct the thermal characterization of the reactor. Different levels of radiation attenuation were employed in the facility, implemented by means of partially transparent radiation screens with various open area fractions.

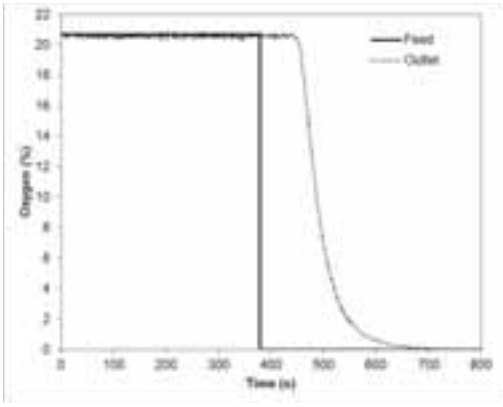

Fig. 12: Oxygen evolution when air is changed to nitrogen

Two tests are performed. A test with attenuation levels of 59%, 50% and 32%, and another test with attenuation levels of 32% and 0%. HFSS is turned off to change the screen attenuation and then it is turned on. Figure 14 shows the temporal evolution of temperatures in cavity, measured in both tests. Temperatures plotted in the figure include those measured at the conical section, the gas reaction zone (measured with two thermocouples), and outer tube wall temperature at the reaction zone. A list of the maximum operating temperatures achieved in the facility is given in Table 2. One of the thermocouples in the reaction zone was damaged during the test with lowest attenuation and data is not shown for it after that time (the maximum operating temperatures of K-type thermocouples is typically 1200 ºC).

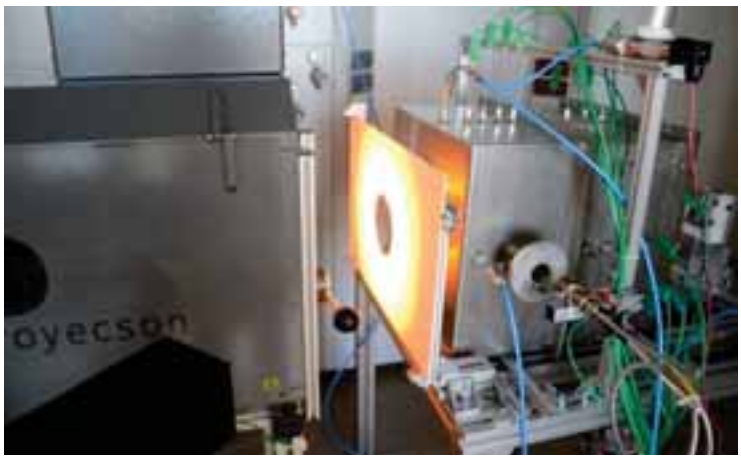

Fig. 13: Setup rotary kiln in front of high flux solar simulator

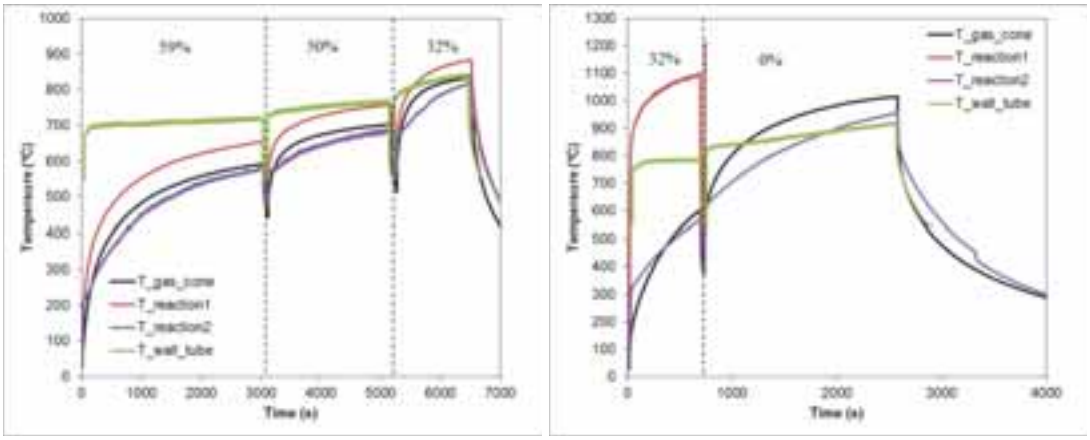

Fig. 14: Temperatures traces: attenuation levels of 59%, 50% and 32% (left); attenuation levels of 32% and 0% (right)

Tab. 2: Maximum temperature achieved in operation for different attenuations (the thermocouple was damaged during te test at 0% attenuation)

Attenuation	T max (ºC)
59%	655
50%	760
32%	1085
0%	>1200

Once the thermal characterization is done, experiments with thermochemical reactions were conducted. Manganese oxide cylindrical pellets (a mixture composed of 85% Mn_3O_4 and 15% Mn_2O_3, mean particle size 3.5 mm) were introduced in the reaction zone of the cavity. Redox reactions are the following:

Oxidation: $4\ Mn_3O_4 + O_2 \rightarrow 6\ Mn_2O_3$ (around 700 ºC)

Reduction: $6\ Mn_2O_3 \rightarrow 4\ Mn_3O_4 + O_2$ (around 950 ºC)

Air was fed while heating the working section in order to produce the complete oxidation of Mn_3O_4. The air supply was changed to nitrogen when temperatures of the reaction zone are higher than 700 ºC (temperature of the oxidation) in order to produce the reduction of Mn_2O_3. Results are showed in Fig. 15, where the full test is represented and reduction area is amplified. When oxygen concentration reaches steady state conditions at temperatures above 700 ºC, the air is changed to pure nitrogen. In this part of the experiment, an increase in the oxygen concentration is observed because of the reduction reaction. In order to study the variation in oxygen concentrations, this is compared to the variation that occurs at ambient temperatures (i.e., without reaction) when air is changed to pure nitrogen. The difference between both curves is due to the oxygen that is released during the reduction reaction.

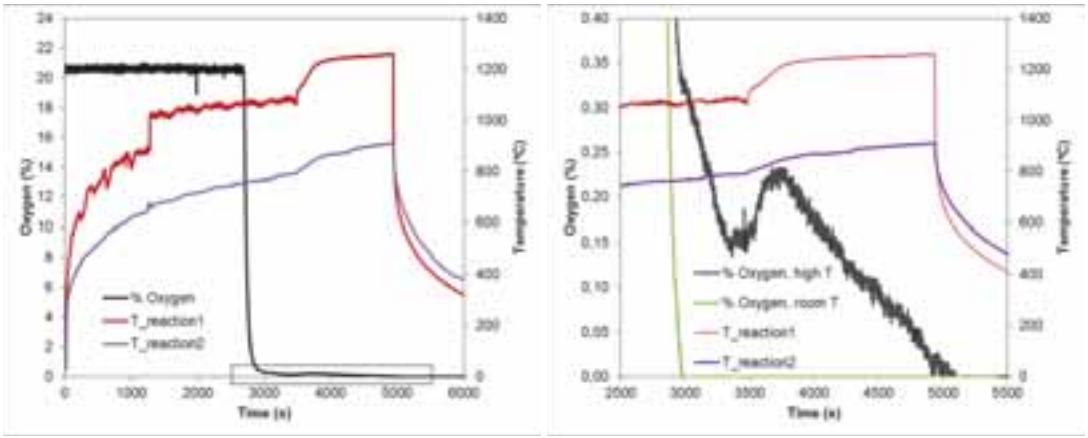

Fig. 15: Temperatures and oxygen concentration evolution, attenuation level of 32%. Full test (left), zoom on reduction reaction (right)

After the experiment, particles were removed from the reactor and analyzed (photographs of them before and after the experiment are shown in Fig. 16). It can be seen that after the tests, particles are brown in color (as opposed to black, initially) and partially worn down at the edges. Figure 17 presents histograms of particle sizes fed and discharged. It is clearly observable that sizes decrease during the test, between 0.2 and 0.4 mm, approximately. X-Ray Diffraction (Fig. 18) confirms that these particles are 100% Mn_3O_4; hence, a full conversion of the initial 15% of Mn_2O_3 is achieved.

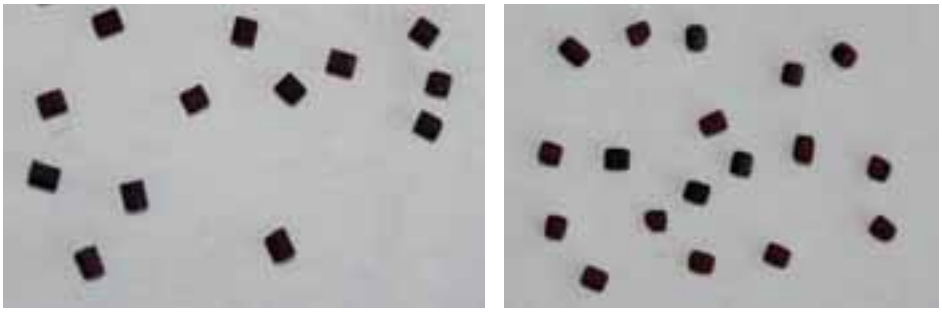

Fig. 16: Particles fed (left), particles discharged (right)

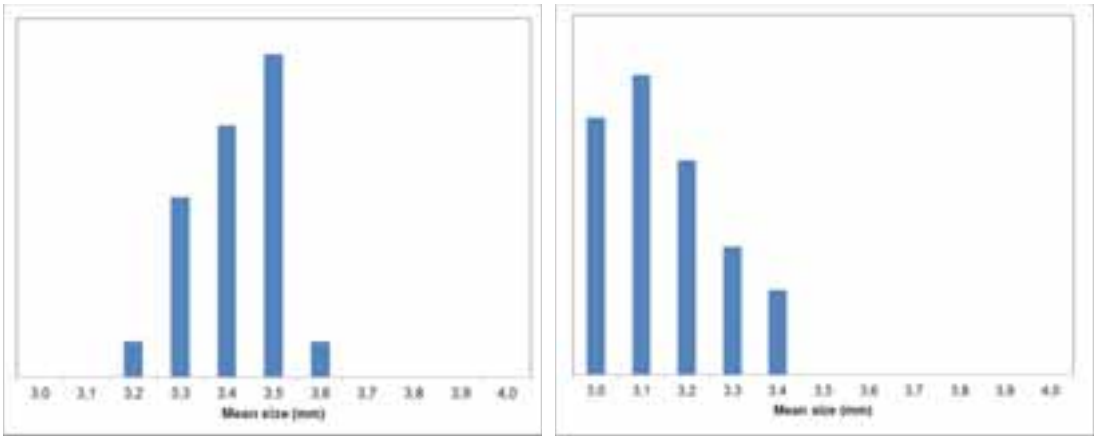

Fig. 17: Mean particle size distributions of particles fed (left) and particles discharged (right)

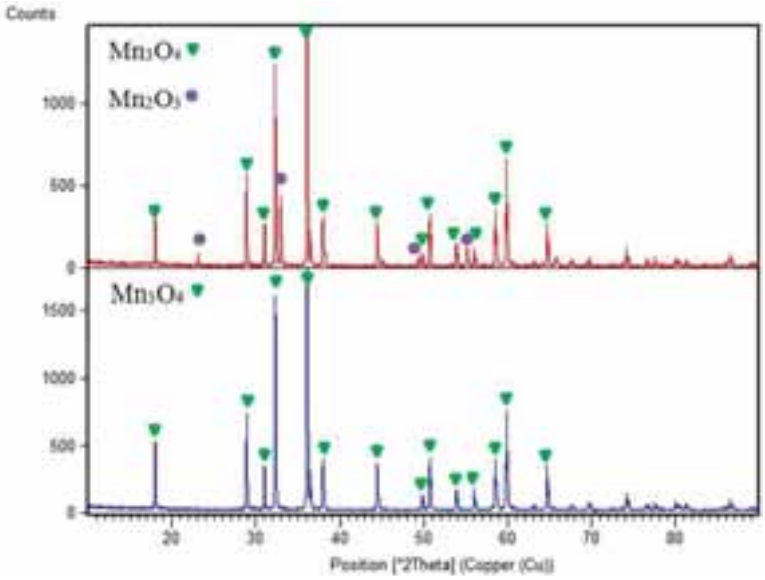

Fig. 18: X-Ray Diffraction results: particles fed (top), particles discharged (bottom)

5. Conclusions

A rotary kiln for experiments in a HFSS have been design, built, simulated and commissioned. The design allows reacting particles to be directly irradiated at high flux and high temperature conditions.

Optical analysis by Monte Carlo ray tracing was conducted to select the optimal position of the reactor relative to the HFSS in order to achieve a total power at the reaction zone of around 1 kW.

A preliminary CFD model was developed for the empty reactor and without rotation. Results indicated that

the maximum temperature was achieved at the reaction zone (1700 K).

Commissioning experiments in the 7kW$_e$ HFSS demonstrated that is possible to reach high temperatures at the reaction zone (1500 K). Thermochemical reaction experiments with manganese oxides (85% Mn_3O_4 y 15% Mn_2O_3) were performed, with air being fed during the heating of the kiln, and nitrogen when temperatures reached 700 ºC. The production of oxygen was measured at high temperatures from the reduction chemical reaction. Discharged material was 100% reduced (Mn_3O_4).

6. References

Alonso, E., Perez-Rabago, C., Licurgo, J., Fuentealba, E., Estrada, C.A., 2015. First experimental studies of solar redox reactions of copper oxides for thermochemical energy storage. Solar Energy. 115, 297-305.

Alonso, E., Romero, M., 2015. Review of experimental investigation on directly irradiated particles solar reactors. Renewable and Sustainable Energy Reviews. 41, 53-67.

COMSOL Multiphysics Version 4.4, COMSOL AB, Stockholm, Sweden, 2013. www.comsol.com

Haueter, P., Moeller, S., Palumbo, R., Steinfeld, A., 1999. The production of zinc by thermal dissociation of zinc oxide- Solar chemical reactor design. Solar Energy. 67, 161-167.

LabView Version 2013, National Instruments Corporation, Austin, USA, 2013. www.ni.com/labview

Meier, A., Bonaldi, E., Cella, G., Lipinski, W., Wuillemin, D., 2004. Design and experimental investigation of a horizontal rotary reactor for the solar thermal production of lime. Energy. 29, 811-821.

Müller, R., Haeberling, P., Palumbo, R., 2006. Further advances toward the development of a direct heating solar thermal chemical reactor for the thermal dissociation of ZnO(s). Solar Energy. 80, 500-511.

Neises, M., Tescari, S., Oliveira, L., Roeb, M., Sattler, C., Wong, B., 2012. Solar-heated rotary kiln for thermochemical energy storage. Solar Energy. 86, 3040-3048.

Romero, M., Steinfeld, A., 2012. Concentrating solar thermal power and thermochemical fuels. Energy & Environmental Science. 5, 9137–9674.

Tescari, S., Neises, M., Oliveira, L., Roeb, M., Sattler, C., Neveu, P., 2013. Thermal model for the optimization of a solar rotary kiln to be used as high temperature thermochemical reactor. Solar Energy. 95, 279-289.

TracePro Version 7.2, Lambda Research Corporation, Littleton, USA, 2012. www.lambdares.com

Acknowledgements

The research leading to these results has been conducted under the grant Plan Nacional ENE2011-29293 funded by the Spanish Ministry of Science and Innovation, which the authors gratefully acknowledge. The collaboration and funding of the regional government of the Community of Madrid and the European Social Fund, through the funding of the project ALCCONES (Storage and Conversion of Concentrating Solar Thermal Energy, S2013/MAE-2985), and the European Union, through the Seventh Framework Research Programme STAGE-STE (Scientific and Technological Alliance for Guaranteeing the European Excellence in Concentrating Solar Thermal Electricity, ENERGY.2013.10.1.10), are also particularly appreciated.